15th CIRP Conference on Modelling of Machining Operations

Sensitivity Analysis of Cryogenic Cooling on Machining of Magnesium Alloy AZ31B-O

Mohamed N.A. Nasr[a,b,*], J.C. Outeiro[c]

[a]*Dept. of Mechanical Engineering, Faculty of Engineering, Alexandria University, Alshatby, Alexandria, 21544, Egypt*
[b]*Dept. of Materials Science & Engineering, Egypt-Japan University of Science & Technology, New Borg El-Arab, Alexandria, 21934, Egypt*
[c]*Arts et Metiers ParisTech, LaBoMaP, Rue Porte de Paris, 71250 Cluny, France*

* Corresponding author. Tel.: +20-3-591-5848; fax: +20-3-590-2715. *E-mail address:* m.nasr@alexu.edu.eg.

Abstract

Improving the corrosion resistance of magnesium alloys has gained special focus in recent years, and cryogenic machining has been one of the successfully used techniques. The current study presents a sensitivity analysis of cryogenic cooling effects on process mechanics, when cutting AZ31B-O magnesium alloy. Finite element modelling was used to simulate orthogonal cutting of AZ31B-O under dry and cryogenic conditions, where different parameters (cutting forces, temperatures, shear angle, chip compression ratio and plastic deformation) were investigated. Also, orthogonal cutting tests were performed on a CNC lathe, under dry and cryogenic conditions, where cryogenic cooling was applied to the clearance side using an LN2 jet.

Peer-review under responsibility of the International Scientific Committee of the "15th Conference on Modelling of Machining Operations

Keywords: Cryogenic machining, Finite element method (FEM), Magnesium, Process mechanics, Turning.

1. Introduction

Surface integrity is a very critical parameter in controlling part performance. It contributes to its mechanical strength, hardness, fatigue life, as well as corrosion resistance [1-3]. Magnesium (Mg) alloys have recently gained special attention as good candidates for automotive and aerospace applications, due to their relatively lightweight [1]. In addition, they are emerging as a strong potential material for biodegradable metallic implants [4,5]. However, one of the main challenges facing their use is their limited corrosion resistance [1,5-7].

Several approaches have been tried in order to improve the corrosion resistance of Mg alloys. This includes the use of different alloying elements, protective coatings and recently by improving the surface integrity of the component [6]. As an example of surface integrity improvements, grain refinement was proved to be effective in improving Mg alloys corrosion resistance [2,6,8,9], as well as their wear resistance [1] and fatigue life [8]. In addition, surface compressive residual stresses (RS) were proved to improve fatigue life [1,8] and corrosion resistance of different materials [1,2,6]. Crystallographic orientation was also found to be an important factor contributing to the corrosion resistance of Mg alloys [1,2]. It is worth mentioning that, the use of coatings is limited in biomedical applications due to possible adverse tissue reactions [5].

Machining, as a severe plastic deformation (SPD) process, has a profound effect on surface integrity. It has been proved to be an effective method for grain refinement; in addition, surface compressive RS could be induced under well-controlled conditions [1,10]. However, the large amount of heat generation may have a detrimental effect on surface integrity, where the thickness of the grain refinement layer is often very thin [6,10], and the possibility of ending up by surface compressive RS decreases [10,11]. In cryogenic machining, cryogenic cooling is typically applied to the clearance side, between the tool flank face and newly machined surface, using a jet of liquid nitrogen (LN2). This lowers the temperature of the tool and workpiece, and consequently improves productivity and tool life [1,12], as

well as surface integrity [6,13]. It has been also proved to improve the corrosion resistance of AZ31B Mg alloy [2,9].

Even though the available literature has shed some light on cryogenic machining of Mg alloys, with special focus on surface integrity [1,2,5,6,9,13-15], some details are still missing. In addition, the use of finite element modelling (FEM) for examining the effects of cryogenic cooling on the machining process has been very limited so far; a few examples could be found in [5,13,15]. Accordingly, the current work presents a sensitivity analysis on cryogenic machining of Mg alloy AZ31B-O, where the effects of cryogenic cooling on different machining parameters (cutting forces, temperatures, shear angle, chip compression ratio and material plastic deformation) are examined. Two-dimensional plane strain finite element (FE) models were built, in order to simulate dry and cryogenic orthogonal cutting of AZ31B-O. For model validation, experimental orthogonal cutting tests were also performed, under dry and cryogenic conditions.

2. Experimental Work

Orthogonal cutting tests were performed on Mg alloy AZ31B-O disks (95 mm in diameter with 3 mm width), using uncoated cemented carbide inserts with the following specifications; normal rake angle of +5º, normal flank angle of 6º, and cutting edge radius (r_n) of 35 μm. A cutting speed of 100 m/min along with uncut chip thickness (h) of 0.1 and 0.2 mm was used. Testing was performed on a CNC lathe under dry and cryogenic cooling conditions. Cryogenic cooling was applied between the newly machined surface and tool flank face, using a jet of LN2 at -196 °C (nozzle diameter of 1 mm and a pressure of 2 bar). Fig. 1 shows the used experimental setup, where cutting forces were measured using a Kistler 9121 dynamometer. A conventional lathe equipped with a quick-stop device was also used, in order to quickly disengage the tool and generate a surface with constant chip thickness.

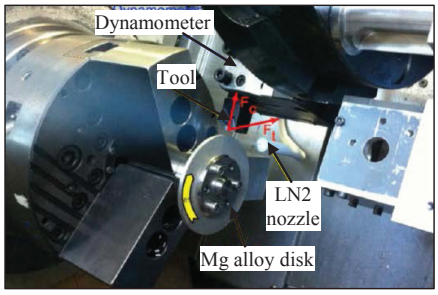

Fig. 1. Experimental setup.

3. Finite Element Modelling (FEM)

3.1. General description

Two-dimensional plane strain Lagrangian FE models were built, using the commercial software ABAQUS/Explicit, in order to simulate orthogonal cutting of Mg alloy AZ31B-O, under dry and cryogenic conditions. Coupled temperature-displacement analysis was used in order to allow for temperature-dependent material properties and heat transfer. Fig. 2 shows the cutting model with the location of cryogenic cooling (clearance side) shown. Cutting conditions (speed, h, r_n, rake and flank angles) are similar to the experimental ones.

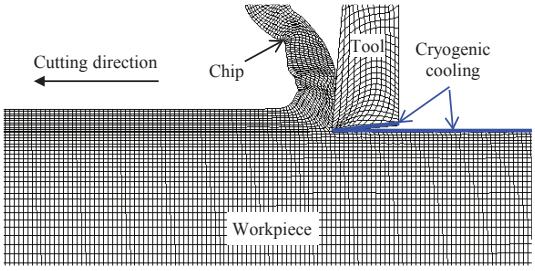

Fig. 2. Cutting model, with the location of cryogenic cooling shown.

3.2. Edge-radius (r_n) effects

The effects of r_n on different process parameters were evaluated, during dry and cryogenic machining. This was done by building an extra model with a sharp-edged tool (r_n = 2 μm), in addition to the one representing the experimental r_n value (35 μm). It is worth mentioning that, based on the available literature [1,3,14], r_n was expected to alter the magnitude of results but not to change their trend. For AZ31B Mg alloy, Pu et al. [1] demonstrated experimentally that the trend of change in cutting forces, temperatures, surface roughness and surface RS, under dry and cryogenic orthogonal cutting, is independent of r_n.

It is important to note that, Lagrangian formulation is more suitable for modelling cutting with sharp-edged tools. This is because of the need for defining a sacrificial layer (parting line), which is hard to predict for honed tools. In the current work, the size of the sacrificial layer when r_n = 35 μm was estimated based on the work presented earlier in [3].

3.3. Cryogenic cooling effects

Cryogenic cooling effects and air convection to the environment were modelled by defining a convection heat transfer coefficient (h_f) and a sink temperature (T_f), for each case. Air convection was defined on all external surfaces, except those used for cryogenic cooling, with a convection heat transfer coefficient (h_{air}) of 10 W/(m^2 °C) [16] and T_f of 20 °C (room temperature). Cryogenic cooling was applied to the clearance side, as shown in Fig. 2. The cryogenic cooling convection coefficient (h_{cryo}) was more difficult to be determined, as it depends on several factors [17]. This is why several values can be found in the literature, varying from 2 to 50 kW/(m^2 °C) [18, 19]. Such values were estimated based on experimental testing or heat transfer calculations. Astakhov [20] proposed the following equation to estimate h_{cryo} in metal cutting:

$$h_{cryo} = \frac{0.20}{b^{0.35} g^{0.33}} \cdot \frac{V_f^{0.65} k_f^{0.67} c_p^{0.33} \gamma_f^{0.33}}{v_f^{0.32}} \quad (1)$$

where; b is the equivalent length (m), g is the gravitational acceleration (m^2/s), and the remaining parameters are properties of the fluid, namely: v_f is the velocity (m/s), k_f is the thermal conductivity (W/m °C), γ_f is the specific weight (kg/m^3), υ_f is the dynamic viscosity (Pa.s) and c_p is the specific heat capacity (J/kg °C). Based on Eq. 1, the value of h_{cryo} was found to be 2 kW/(m^2 °C) for the current conditions. However, different values were used for the sensitivity analysis, namely: 2, 20, 200 and 2000 kW/(m^2 °C). A T_f value of -196 °C was used, representing the temperature of LN2.

During machining, h_{cryo} was applied to the workpiece newly machined surface as it grows in size. This was done by creating sequential time-dependent virtual surfaces, along the newly machined surface as it grows, with h_{cryo} assigned to them. Since a Lagrangian cutting model starts with no exposed machined surface, it was inevitable to wait certain duration (delay time) till an initial exposed surface is formed. In the current work, an initial surface with length of 100 µm was assumed to be reasonable; this corresponds to a delay period of $6x10^{-5}$ seconds (3% of the total cutting time). It also represents a case where the LN2 jet cannot effectively get in good contact with the machined surface close to the tool tip. This could be the case especially with high cutting speeds and low thermal diffusivity. Heat radiation was neglected as it is negligible compared to conduction and convection.

3.4. Contact definitions

Surface-to-surface contact pairs were used for defining contacts between the tool and workpiece. The tool-workpiece friction was modelled using the simple Coulomb model, with a shear limit of 150/√3 MPa [13]. The friction coefficient was determined experimentally using a special designed pin-on-disk experimental setup, and found to be 0.12 under dry and cryogenic conditions. The pin was made of the same material as the tool, fixed to the tool holder of a CNC lathe, and was sliding against a plate of AZ31B-O alloy that was fixed to the spindle. The pin described a spiral path over the plate at a constant velocity. The applied contact pressure and sliding speed were similar to those generated during machining. The pressure was calculated based on the measured forces, obtained from orthogonal cutting tests. The frictional heat was equally split between the tool and chip/workpiece, based on the heat partition coefficient (P) given by Eq. 2. Eq. 2 defines the fraction of heat (P) flowing into surface (1) when in contact with surface (2).

$$P = \frac{H_1}{H_1 + H_2} \quad (2)$$

Where; $H = \sqrt{k\,\rho\,c_p}$, k is the thermal conductivity (W/m °C), ρ is the density (kg/m^3) and c_p is the specific heat capacity (J/kg °C).

3.5. Workpiece material properties and chip generation

The physical properties of AZ31B-O were defined as functions of temperature, as obtained from [5]. Plasticity was modelled using the well-known Johnson–Cook (J–C) constitutive model, where Table 1 presents its parameters for AZ31B-O, as obtained from [21]. The melting and reference temperatures of AZ31B-O are 650 °C and 25 °C, respectively [21]. For chip separation, material failure was predicted based on the J-C cumulative damage law. The corresponding J-C damage parameters ($D1$ – $D5$) for AZ31B-O were obtained from [21], and presented in Table 2.

Table 1. AZ31B-O J-C constitutive model parameters [21].

A (MPa)	B (MPa)	n	C	$\dot{\varepsilon}_0$ (s^{-1})	m
172	360.73	0.45592	0.092	1	0.95

Table 2. AZ31B-O J-C cumulative damage parameters (unit-less) [21].

$D1$	$D2$	$D3$	$D4$	$D5$
-0.35	0.6025	-0.4537	0.206	7.2

4. Results and Discussion

The current section presents the effects of cryogenic (Cryo) cooling on cutting forces, temperatures, shear angle, chip compression ratio (CCR) and material plastic deformation. Four cases have been examined; h_{cryo} = 2, 20, 200, 2000 kW/(m^2 °C), which are referred to hereafter as h_1, h_2, h_3, h_4.

4.1. Cutting forces and edge-radius (r_n) effects

Table 3 presents the predicted effects of r_n on cutting (F_c) and thrust force (F_t) components as well as maximum workpiece temperature (T_{max}), during dry and cryogenic machining. For cryogenic conditions, h_4 results are presented. Experimental (Exp.) cutting forces are also presented, but no temperature measurements were performed. Experimentally, an increase in F_c and F_t was noticed with cryogenic conditions, which could be attributed to the slightly lower temperatures in the chip formation zone, as shown below. The increase in F_c was more significant when h = 0.2 mm. On the other hand, the increase in F_t was less obvious at higher h values. Both FE models (r_n = 35 µm and r_n = 2 µm) also predicted a slight increase in F_c with cryogenic cooling; however, they both overestimated it especially the former. The over prediction of F_c could be attributed to the used J-C constitutive and fracture model parameters, as well as the friction model. Both models also estimated a slight increase in F_t with cryogenic cooling, with a significant underestimation by the latter and a slight overestimation by the former.

Table 3. Effect of cryogenic cooling and r_n on forces and T_{max}.

Case	Parameter	h = 0.1 mm		h = 0.2 mm	
		Dry	*Cryo*	Dry	*Cryo*
Exp.	Fc (N/mm)	52	54	80	111
	Ft (N/mm)	35	41	44	45
r_n = 35 µm	T_{max} (°C)	333	328	318	312
	Fc (N/mm)	143	157	261	279
	Ft (N/mm)	42	45	39	55
r_n = 2 µm	T_{max} (°C)	302	295	302	287
	Fc (N/mm)	78	103	176	193
	Ft (N/mm)	3	3	7	6

Table 4 presents the effects of four different cryogenic cooling rates (h_1 – h_4) on F_c, for r_n = 2 µm, as an example. In general, cryogenic cooling resulted in higher F_c, with no significant differences between different cooling rates. The only exception was when h = 0.1 mm, where h_1 conditions had almost the same F_c as dry cutting.

Table 4. Effect of cryogenic cooling on predicted F_c (r_n = 2 µm).

h (mm)	Dry	Cryogenic			
		h1	*h2*	*h3*	*h4*
0.1	78	76	101	105	103
0.2	176	191	196	195	193

Fig. 3 shows the workpiece temperature distribution during h_4 cryogenic cutting when h = 0.1 mm, as an example, for both r_n values. No significant difference could be noticed in the chip formation zone; only a slight drop in T_{max} (located in the secondary shear zone) was found with cryogenic cooling, as shown in Table 3. Also, slightly higher temperatures were generated in the machined surface with larger r_n values. However, as expected, this was limited to the region right underneath the tool tip and diminished with cryogenic cooling. Finally, it is important to note that, the effects of cryogenic cooling on forces and temperatures followed the same trend regardless of r_n. In other words, r_n only altered the magnitude of change but did not change the trend. Accordingly, only the results of r_n = 2 µm are presented below.

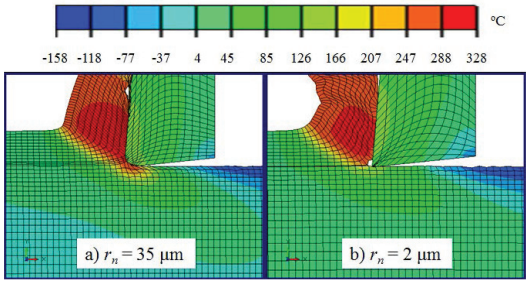

Fig. 3. Effect of r_n on workpiece temperature (h = 0.1 mm & h_4 conditions).

4.2. Workpiece temperatures

The current section focuses on the effects of cryogenic cooling on workpiece temperatures. Fig. 4 shows the temperature distribution during cryogenic (h_4) machining, for r_n = 2 µm and h = 0.1 mm, as an example. Fig. 5 (a) focuses on the temperature distribution in the cutting zone, for the same conditions. No significant differences could be found in the chip formation zone and tool-chip contact. The same trend was found for h = 0.2 mm. However, temperature contours are clearly different away from the chip generation region, particularly in the machined surface and tool flank face, as shown in Fig. 5 (b). It is important to note that, the insignificant effect of cryogenic cooling on the chip formation zone temperatures is attributed to where the LN2 jet was applied (clearance side), which limits its accessibility to that zone, as explained earlier. Moreover, the current model does not take into account the precooling effect from previous cuts.

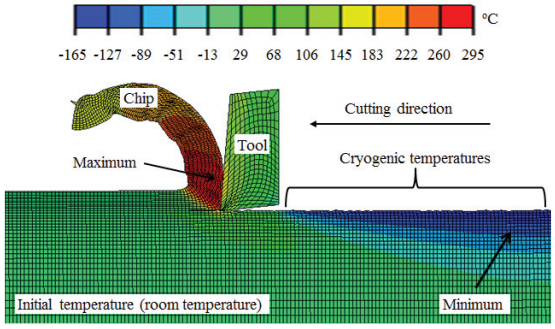

Fig. 1. Temperature distribution (h_4 conditions, r_n = 2 µm & h = 0.1 mm).

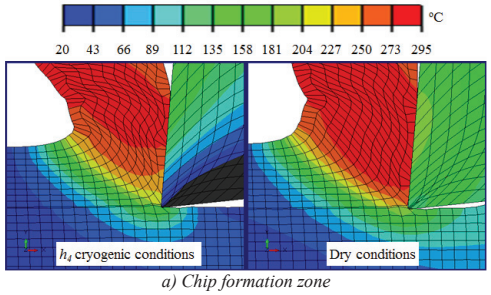

a) Chip formation zone

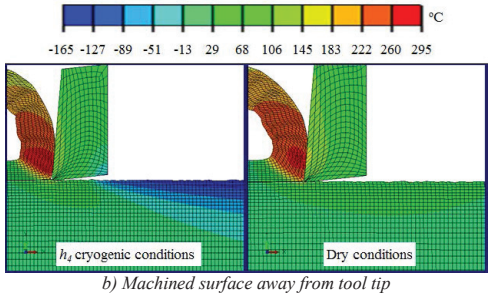

b) Machined surface away from tool tip

Fig. 2. Temperature distribution: (a) chip formation zone; (b) far from tool tip (r_n = 2 µm & h = 0.1 mm; note: dark grey region is below room temperature).

Table 5 presents the average temperature in the chip formation zone when r_n = 2 µm, where a maximum drop of 40 °C was achieved for the lower h value. However, insignificant change was noticed for the higher h value. The reason why cryogenic cooling effects were less evident at higher h values could be explained in terms of heat evacuation via chip movement. With higher h value, the chip is more capable of carrying away a larger portion of the generated heat. It is important to note that, one would expect lower temperatures when dry cutting using higher h because of the same reason.

Table 5. Average temperature (°C) of chip formation zone (r_n = 2 µm).

h (mm)	Dry	*h1*	*h2*	*h3*	*h4*
0.1	271	268	265	250	231
0.2	252	254	252	245	245

The workpiece temperatures at tool–chip contact zone are presented in Fig. 6, which focuses on three temperatures; 1) maximum, 2) start of contact (tool tip), and 3) end of contact. Slight drop in temperatures was noticed due to cryogenic cooling; such drop was more evident at the tool tip, which is the closest to the LN2 jet.

Finally, Fig. 7 presents the workpiece temperature distribution right underneath the tool tip. Cooling effects were found to be limited to the near-surface layer (about 150 µm), with a maximum drop of about 30 °C. The limited temperature drop is mainly attributed to the assumed delay time when applying cryogenic cooling effects, which is equivalent to a length of 100 µm, as explained earlier. Cryogenic temperatures were clearly achieved far from the tool tip, at a distance larger than 100 µm, as shown in Fig. 4 and Fig. 5 (b).

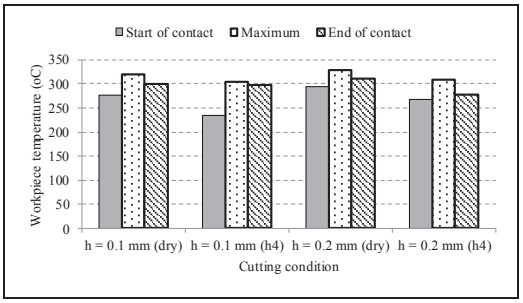

Fig. 3. Workpiece temperatures at tool–chip contact zone (r_n = 2 µm).

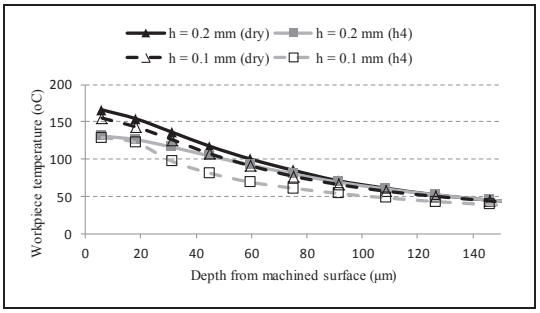

Fig. 4. Workpiece temperatures underneath the tool tip (r_n = 2 µm).

4.3. CCR, shear angle and tool-chip contact length

The chip-tool contact length (l_c) was predicted for different cases, and was found to slightly decrease with cooling effects for both r_n values. This was more evident with higher h values, and could be attributed to the slightly lower temperatures along the tool rake face that would result in a smaller sticking region. The experimental l_c value was calculated based on the chip compression ratio (CCR), as per Eq. 3 for CCR < 4 [20], which is the current case. It was also predicted by the models. The shear angle (Φ) was calculated using Eq. 4, where γ is the normal rake angle.

$$l_c = t_1 * CCR^{1.5} \quad (3)$$

$$tan(\emptyset) = \frac{cos(\gamma)}{CCR - sin(\gamma)} \quad (4)$$

Table 6 summarizes the current results of l_c, CCR and Φ for r_n = 2 µm, as an example. As shown, cryogenic cooling did not have clear effects on Φ. For h = 0.1 mm, Φ started to decrease with cooling, and finally increased for h_4 conditions. The opposite took place for h = 0.2 mm. No clear reason could be found, and such differences could be due to numerical errors. Nevertheless, the predicted Φ values are close to those found experimentally, and those reported in [1].

Table 6. Chip-tool contact length, CCR and shear angle (Φ).

h (mm)	Item	Exp.		FEM				
		Dry	Cryo	Dry	Cryo			
					h1	*h2*	*h3*	*h4*
0.1	l_c (mm)	0.18	0.19	0.21	0.17	0.18	0.18	0.19
	CCR	1.48	1.55	1.70	1.80	1.85	1.85	1.60
	Φ (°)	35.6	34.3	31.7	30.2	29.5	29.5	33.4
0.2	l_c (mm)	N/A	N/A	0.39	0.39	0.36	0.31	0.32
	CCR	N/A	N/A	1.85	1.60	1.65	1.80	1.75
	Φ (°)	N/A	N/A	29.5	33.4	32.5	30.2	30.9

It is important to note that, the current model could not fully predict chip segmentation, which was the case experimentally. Even though signs of segmentation initiation were very obvious, as shown in Fig. 8, the process was not fully predicted. This could be attributed to the used fracture model, which may require future improvements.

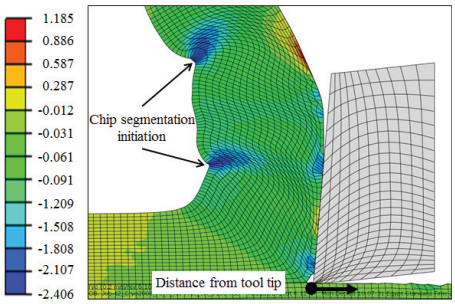

Fig. 5. Plastic shear strain (r_n = 2 µm, h = 0.2 mm & *h4* conditions).

4.4. Material plastic deformation

Examining the effects of cryogenic cooling on plastic deformation in different regions, no significant effects were found in the chip formation zone and along the tool-chip contact area. This is attributed to the limited effects on temperature distribution in both regions. On the other hand, cryogenic cooling affected the plastic strain distribution in the machined surface. Table 7 presents the plastic strain in cutting direction (PE11) and temperature ($T_{surface}$) of the machined surface, at different distances from the tool tip (as indicated by the arrow in Fig. 8). For a better evaluation, results were averaged over distances of 100 µm. As shown, cryogenic cooling resulted in higher tensile PE11. It is worth mentioning that, the opposite took place right underneath the

tool; however, cooling effects were not effective in that region, as explained earlier.

Table 7. Cryogenic effects (h_4) on $T_{surface}$ and PE11 (r_n = 2 μm, h = 0.2 mm).

Distance from tool	Dry conditions		Cryogenic h_4 conditions	
tip (see Fig. 8)	$T_{surface}$ (°C)	PE11	$T_{surface}$ (°C)	PE11
1st 100 μm	150	0.010	95	0.003
2nd 100 μm	100	- 0.018	- 50	0.012

5. Conclusions and Outlook

A sensitivity analysis has been performed on how cryogenic cooling affects the machining of Mg alloy AZ31B-O; however, precooling effects (from previous cuts) were not considered. FEM has been used, where different values have been assigned to the cryogenic convection coefficient of heat transfer (h_{cryo}), covering the range from 2 kW/(m^2°C) to 2000 kW/(m^2°C). Based on the current results, the following conclusions were drawn.

1. Cryogenic cooling results in lower machined surface and tool rake temperatures. This is basically attributed to the fact that the cooling LN2 jet is applied to the clearance side;
2. Cryogenic cooling results in a slightly shorter chip-tool contact length, which could be attributed to the slightly lower tool temperatures that would result in a smaller sticking region;
3. The effect of cryogenic cooling on shear angle is not very clear;
4. Cryogenic cooling tends to induce higher tensile plastic strain in the machined surface;
5. Cryogenic machining generates slightly higher cutting forces. This is attributed to the slightly lower primary shear zone temperatures; i.e., less softening effects;
6. As the magnitude of h_{cryo} increases (within the studied range), the following was found: a) the temperature of the machined surface dropped significantly, but that in the chip formation zone only slightly dropped; b) the shear angle and chip compression ratio showed no significant change; c) the contact length was almost unaffected for the small uncut chip thickness (0.1 mm), but it decreased for the large uncut chip thickness (0.2 mm); and finally, d) the cutting force component slightly dropped. Therefore, it could be concluded that the value of h_{cryo} has insignificant effects on the cutting mechanics *per se*; however, it would have strong effects on surface integrity.

An improved model is to be developed in order to better simulate the process, and better predict chip segmentation.

References

[1] Pu Z, Outeiro JC, Batista AC, Dillon Jr OW, Puleo DA, Jawahir IS. Enhanced surface integrity of AZ31B Mg alloy by cryogenic machining towards improved functional performance of machined components. Int J Mach Tool Manu 2012; 56: 17-27.

[2] Pu Z, Song GL, Yang S, Outeiro JC, Dillon Jr OW, Puleo DA, Jawahir IS. Grain refined and basal textured surface produced by burnishing for improved corrosion performance of AZ31B Mg alloy. Corrosion Science 2012; 57: 192-201.

[3] Nasr MNA, Ng EG, Elbestawi M. Modelling the effects of tool-edge radius on residual stresses when orthogonal cutting AISI-316L. Int J Mach Tool Manu 2007; 47: 401-11.

[4] Witte . The history of biodegradable magnesium implants: a review. Acta Biomaterialia 2010; 6: 1680–92.

[5] Pu Z, Umbrello D, Dillon Jr. OW, Lu T, Puleo DA, Jawahir IS. Finite element modelling of microstructural changes in dry and cryogenic machining of AZ31B magnesium alloy. J. of Mfg. Processes 2014; 16: 335–43.

[6] Outeiro JC, Batista AC, Marques MJ. Residual stresses induced by dry and cryogenic cooling during machining of AZ31B magnesium alloy. Adv. Mater Research 2014; 996: 658-63.

[7] Denkena B, Lucas A. Biocompatible magnesium alloys as absorbable implant materials – adjusted surface and subsurface properties by machining processes. CIRP Ann - Manuf Techn 2007; 56: 113-16.

[8] Wang H, Estrin Y, Fu H, Song G, Zuberova Z. The effect of pre-processing and grain structure on the bio-corrosion and fatigue resistance of Magnesium alloy AZ31B. Adv. Eng. Mater. 2007; 9: 967–72.

[9] Pu Z, Yang S, Song GL, Dillon Jr OW, Puleo DA, Jawahir IS. Ultrafine-grained surface layer on Mg–Al–Zn alloy produced by cryogenic burnishing for enhanced corrosion resistance. Scripta Materialia 2011; 65: 520–23.

[10] Jawahir IS, Brinksmeier E, M'Saoubi R, Aspinwall DK, Outeiro JC, Meyer D, Umbrello D, Jayal AD. Surface integrity in material removal processes: recent advances. CIRP Ann - Manuf Techn 2011; 60: 603-26.

[11] Nasr MNA, Ng EG, Elbestawi M. Effects of strain hardening and initial yield strength on machining-induced residual stresses. J Eng Mater – T ASME 2007; 129: 567-79.

[12] Nasr MNA, Balbaa M, Elgamal H. Modelling machining-induced residual stresses after laser-assisted turning of steels. Adv Mater Research 2014; 996: 622-7.

[13] Outeiro JC, Rossi F, Fromentin G, Poulachon G, Germain G, Batista AC. Process mechanics and surface integrity induced by dry and cryogenic machining of AZ31B-O magnesium alloy. Procedia CIRP 2013; 8: 486-91.

[14] Pu Z, Outeiro JC, Batista AC, Dillon Jr OW, Puleo DA, Jawahir IS. Surface integrity in dry and cryogenic machining of AZ31B Mg alloy with varying cutting edge radius tools. Procedia Eng 2011; 19: 282-87.

[15] Pu Z, Umbrello D, Dillon Jr OW, Jawahir IS. Finite element simulation of residual stresses in cryogenic machining of AZ31B Mg alloy. Procedia CIRP 2014; 13: 282–7.

[16] Nasr MNA, Ng EG, Elbestawi M. A modified time-efficient FE approach for predicting machining-induced residual stresses. Finite Elements in Analysis & Design 2007: 44; 149-61.

[17] Barron RF, Nellis G, Pfotenhauer JM. Cryogenic heat transfer, CRC Press, 1999.

[18] Richards DG, Prangnell PB, Withers PJ, Williams SW, Morgan S. Simulation of the effectiveness of dynamic cooling for controlling residual stresses in friction stir welds, 7th Int. Friction Stir Welding Symposium, 2008.

[19] Hong SY, Ding Y. Cooling approaches and cutting temperatures in cryogenic machining of Ti-6Al-4V. Int J Mach Tool Manu 2001; 41: 1417-37.

[20] Astakhov VP. Tribology of metal cutting. 1st ed. Oxford: Elsevier; 2006.

[21] Feng F, Huang S, Meng Z, Hu , Lei Y, Zhou M, Yang Z. A Constitutive and fracture model for AZ31B Magnesium alloy in the tensile state. Materials Science & Engineering 2011; A594: 334–43.